

See discussions, stats, and author profiles for this publication at: <https://www.researchgate.net/publication/261767584>

# Polydiacetylene-Enclosed Near-Infrared Fluorescent Semiconducting Polymer Dots for Bioimaging and Sensing

ARTICLE in ANALYTICAL CHEMISTRY · APRIL 2014

Impact Factor: 5.64 · DOI: 10.1021/ac404237q · Source: PubMed

---

CITATIONS

13

---

READS

21

## 5 AUTHORS, INCLUDING:



Ya-Chi Huang

National Sun Yat-sen University

4 PUBLICATIONS 27 CITATIONS

[SEE PROFILE](#)



Yang-Hsiang Chan

National Sun Yat-sen University

30 PUBLICATIONS 849 CITATIONS

[SEE PROFILE](#)

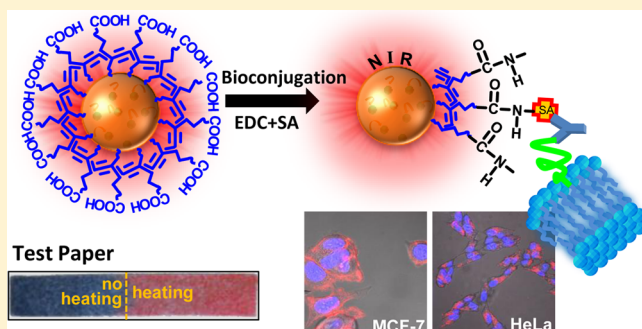
# Polydiacetylene-Enclosed Near-Infrared Fluorescent Semiconducting Polymer Dots for Bioimaging and Sensing

Pei-Jing Wu, Shih-Yu Kuo, Ya-Chi Huang, Chuan-Pin Chen, and Yang-Hsiang Chan\*

Department of Chemistry, National Sun Yat-sen University, 70 Lien Hai Road, Kaohsiung, Taiwan 80424

Supporting Information

**ABSTRACT:** Semiconducting polymer dots (P-dots) recently have emerged as a new type of ultrabright fluorescent probe with promising applications in biological imaging and detection. With the increasing desire for near-infrared (NIR) fluorescing probes for *in vivo* biological measurements, the currently available NIR-emitting P-dots are very limited and the leaching of the encapsulated dyes/polymers has usually been a concern. To address this challenge, we first embedded the NIR dyes into the matrix of poly[(9,9-diethylfluorene)-co-2,1,3-benzothiadiazole-co-4,7-di(thiophen-2-yl)-2,1,3-benzothiadiazole] (PF-BT-DBT) polymer and then enclosed the doped P-dots with polydiacetylenes (PDAs) to avoid potential leakage of the entrapped NIR dyes from the P-dot matrix. These PDA-enclosed NIR-emitting P-dots not only emitted much stronger NIR fluorescence than conventional organic molecules but also exhibited enhanced photostability over CdTe quantum dots, free NIR dyes, and gold nanoclusters. We next conjugated biomolecules onto the surface of the resulting P-dots and demonstrated their capability for specific cellular labeling without any noticeable nonspecific binding. To employ this new class of material as a facile sensing platform, an easy-to-prepare test paper, obtained by soaking the paper into the PDA-enclosed NIR-emitting P-dot solution, was used to sense external stimuli such as ions, temperature, or pH, depending on the surface functionalization of PDAs. We believe these PDA-coated NIR-fluorescing P-dots will be very useful in a variety of bioimaging and analytical applications.



Optical imaging techniques with fluorescence microscopy have been widely used to investigate biological processes in living systems due to their high temporal and/or spatial resolution.<sup>1–3</sup> Since the advances of fluorescence image-guided surgery<sup>4</sup> and its first in-human results for ovarian cancer treatment<sup>5</sup> that can greatly improve intraoperative staging and debulking efforts in cytoreductive surgery, it is prerequisite to develop photostable and highly bright fluorescent agents. Recently, the development of new fluorescent probes with emission in the near-infrared (NIR) region (650–900 nm) has facilitated enormous advances in biological imaging and clinical diagnosis because of their minimal photodamage to biological specimens, low interference from autofluorescence in biological tissues, less scattering in turbid media, and deeper tissue penetration.<sup>6,7</sup> Although conventional organic dyes are the most prevalent NIR fluorescent markers used for general biological studies, several challenges such as rapid photo-bleaching, insufficient brightness, usually poor water solubility, and small Stokes shift are often encountered, which have limited their applications in high-sensitivity imaging, long-term monitoring, and high-throughput assays.

Nanoparticle-based fluorescent probes, therefore, have been developed in which a central, nonfluorescent matrix (e.g., latex, polymer, or silica) is employed to trap NIR dyes.<sup>8–11</sup> However, these optically inert matrixes simply function as carriers and/or surface modifiers and thus greatly limit the potential brightness

and optical functionality of the final nanoparticle probe. Besides, in many cases, such as under physiological conditions, leaching of the embedded dyes from the matrix has been an issue.<sup>12,13</sup> Recently, upconversion nanoparticles have also been widely studied owing to their unique optical properties.<sup>14</sup> Other types of nanoparticle-based fluorescent markers such as inorganic semiconductor nanocrystals (i.e., quantum dots) have also attracted much attention in the past decades owing to their large effective Stokes shift, broad absorption with narrow emission, and improved brightness and photostability over conventional organic dyes.<sup>15–19</sup> However, the potential release of the inorganic component (e.g., cadmium and selenium),<sup>19,20</sup> difficulties in tailoring the surfaces of quantum dots (QDs),<sup>18,21</sup> and the stochastic blinking phenomenon<sup>22</sup> might impede their use for *in vivo* clinical applications.<sup>23–25</sup> Therefore, the exploration of NIR-emitting nanoparticle-based probes that can offer high brightness, good photostability, and biocompatibility is intensely needed.

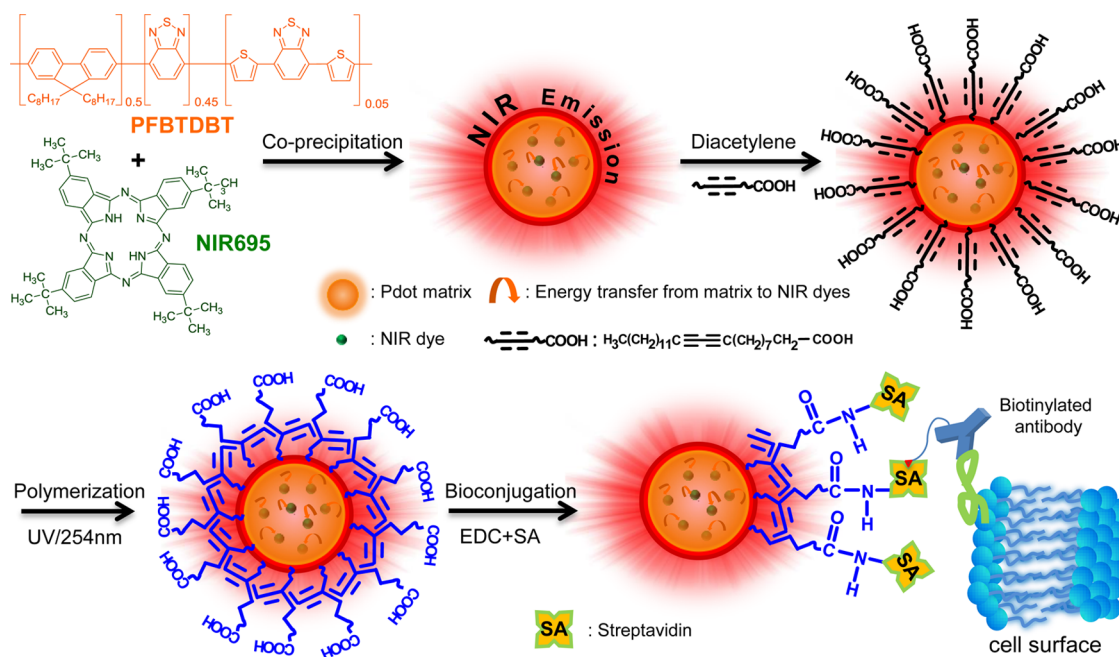
Recently, semiconducting polymer dots (P-dots) have emerged as a new class of promising fluorescent nanoprobes that exhibit excellent fluorescence brightness, good photo-

Received: December 18, 2013

Accepted: April 21, 2014

Published: April 21, 2014

**Scheme 1.** Schematic Illustration of Preparation of PDA-Enclosed NIR Dye-Doped P-Dots and Subsequent Bioconjugation for Specific Cellular Targeting<sup>a</sup>



<sup>a</sup>First, semiconducting polymer PF-BT-DBT and NIR dyes (NIR695 as an example in this scheme) were mixed together in THF and then co-precipitated in water under vigorous sonication to form NIR dye-doped PF-BT-DBT P-dots. Diacetylenes in THF were then injected into P-dot aqueous solution under sonication to form a coating layer of diacetylenes on P-dots. After another vigorous sonication for 10 min, annealing at 60 °C for 30 min, and cooling at 4 °C for 2 h in sequence, the resulting P-dot solution was then polymerized by exposure to a 254 nm UV lamp. The PDA-enclosed NIR dye-embedded PF-BT-DBT P-dots were subsequently conjugated to streptavidin via EDC-catalyzed coupling for specific cellular targeting studies.

stability, high radiative rate, facile surface functionalization, and low cytotoxicity.<sup>26–34</sup> Moreover, the good biocompatibility and facile surface functionalization of P-dots have rendered them extremely useful for a number of applications both *in vitro* and *in vivo*.<sup>6,35–46</sup> Despite this progress, the development of bright NIR-emitting P-dots remains a significant challenge because of the serious self-quenching and reabsorption phenomena of polymer fluorescence upon condensation into a P-dot form. Recently, several strategies have been developed to tackle the above-mentioned challenge. For example, Jin et al.<sup>6</sup> doped the NIR dye silicon 2,3-naphthalocyanine bis(trihexylsilyloxide) into a matrix of poly(9,9-diptylfluorene-*co*-benzothiadiazole) (PF-BT) P-dots. The efficient energy transfer from PF-BT to NIR dye allows them to improve the fluorescence brightness of the NIR dye. In this study, however, ca. 50% (*w/w*) of the amphiphilic, nonfluorescent polymer PS-PEG-COOH [where PS = polystyrene and PEG = poly(ethylene glycol)] was also blended into each individual P-dot in order to prevent leakage of the encapsulated dyes from the P-dot matrixes. This greatly reduces the single-particle brightness of the resulting P-dots and limits their biological applications. Similarly, Zhang et al.<sup>47</sup> mixed more than three types of polymers together at optimized molar ratio inside a P-dot where the NIR emission could be achieved via cascade Förster resonance energy transfer. In this work, specific cell labeling by use of these NIR-emitting P-dots has been demonstrated. However, the potential leakage of the embedded polymers remains a concern that might largely affect the photophysical properties of P-dots.<sup>42</sup> Besides, laborious and time-consuming work is required for the synthesis of polymers with different emission wavelengths.

To address the above-mentioned challenges, here we report a facile, versatile, and scalable strategy (Scheme 1) in which the NIR-emitting dyes are doped into poly[(9,9-diptylfluorene)-*co*-2,1,3-benzothiadiazole-*co*-4,7-di(thiophen-2-yl)-2,1,3-benzothiadiazole] (PF-BT-DBT) polymer and then encompassed by a layer of carboxyl-terminated polydiacetylene (PDA). Specifically, we first examined several different NIR dyes (Figure S1, Supporting Information) with various doping concentrations to achieve the optimal brightness of dye dopant by taking advantage of the amplified energy transfer<sup>27</sup> from the excited P-dot matrix to the acceptor NIR dyes located in close proximity. After the formation of NIR P-dots, we enclosed the surface of P-dots with carboxyl-functionalized diacetylenes (DAs) and then polymerized these DAs via topochemical 1,4-addition<sup>48–57</sup> in an effort to “seal” the embedded NIR dyes. This PDA layer also provided the carboxylate groups that enabled further bioconjugation for specific cellular targeting or functionalization for sensing purposes. Benefiting from the strong absorption of PDAs and the high fluorescence of P-dots, we also designed a dual-responsive colorimetric and fluorescent sensing platform and performed a proof-of-concept experiment. This methodology demonstrated that the encapsulated polymers and the layer of PDA not only functioned as a carrier and a surface modifier but also greatly enhanced the fluorescent properties of the embedded NIR dyes that can be readily employed for a variety of applications. We believe this work has demonstrated the promising applicability of these PDA-wrapped NIR-emitting P-dots in a wide range of cellular imaging and diagnostic studies.

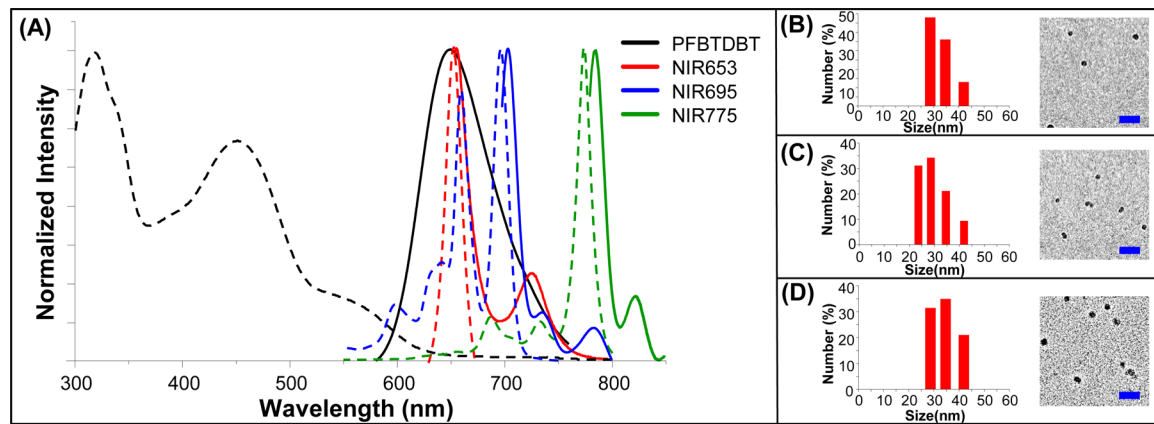


**Figure 1.** (A) UV-visible and fluorescence spectra of PF-BT-DBT P-dots in water (black lines), free NIR653 in tetrahydrofuran (THF) (red lines), free NIR695 in THF (blue lines), and free NIR775 in THF (green lines). Dashed lines represent excitation spectra, while solid lines show corresponding emission spectra. (B) (Left) Hydrodynamic diameters (average diameter was  $\sim 33$  nm) measured by dynamic light scattering (DLS) and (right) transmission electron microscopy (TEM) image of PDA-coated NIR653-PF-BT-DBT P-dots. (C) (Left) Hydrodynamic diameters (average diameter was  $\sim 29$  nm) measured by DLS and (right) TEM image of PDA-coated NIR695-PF-BT-DBT P-dots. (D) (Left) hydrodynamic diameters (average diameter was  $\sim 34$  nm) measured by DLS and (right) TEM image of PDA-coated NIR775-PF-BT-DBT P-dots. Scale bars are 100 nm.

## RESULTS AND DISCUSSION

Our aim was to develop a NIR-emitting P-dot that exploited highly efficient energy transfer from a polymer to NIR dyes that were embedded inside the P-dot. Functionalization of P-dots was achieved by enclosing the dye-doped P-dots with carboxyl-terminated PDA so that they could be tagged with biological molecules for specific cellular targeting applications.

**Selection and Optimization of Polymer–Dye Pair.** In an effort to enable efficient intraparticle energy transfer from the excited polymer matrix to the embedded dyes, first we need to select a good light-harvesting polymer as the donor. To facilitate an efficient energy transfer such as Förster resonance energy transfer (FRET), substantial spectral overlap between the emission spectrum of the selected polymer and the absorption spectrum of the NIR dyes is required. Therefore, an ideal donor here is a polymer that can emit in the deep-red region because most of NIR dyes absorb largely in the deep-red to NIR regions. To date, PF-BT-DBT polymer is one of the brightest deep-red-emitting polymers in the field of organic light-emitting diodes, but its fluorescence quantum yield drops significantly (less than 10%) while condensed into a P-dot form due to the self-quenching of DBT emission at increased concentrations.<sup>36</sup> As a trade-off, we incorporated a DBT molar ratio of only 5% into the PF-BT polymer (Scheme S1, Supporting Information) to achieve a neat 650 nm emission with a quantum yield of 30% in a P-dot form. We then screened a number of NIR dyes by coprecipitation method and found that NIR653, NIR695, and NIR775 offered better performance among those dyes (Figure S1, Supporting Information).

**Preparation of NIR Dye-Encapsulated P-dots.** Once we identified the polymer–dye pair, we wanted to encapsulate NIR dyes into the polymer matrix. Scheme 1 illustrates our strategy for preparing NIR-emitting P-dots by embedding NIR dyes into the matrix of PF-BT-DBT P-dot via the nanoprecipitation method. Due to the hydrophobic properties of NIR653, NIR695, and NIR775, they were apt to be encapsulated inside the hydrophobic PF-BT-DBT P-dot core. Although the presence of hydrophobic interactions between the P-dot matrix and the NIR dyes might prevent leakage of the doped dyes, the long-term optical stability and demand for further functional-

ization for sensing or bioimaging applications remain challenging for this type of P-dot. Therefore, we covered a layer of carboxyl-functionalized DAs, 10,12-pentacosadiynoic acid, onto the surface of the dye-doped P-dots and then polymerized the DAs by illuminating the solution with a 254 nm ultraviolet light under nitrogen atmosphere. The relative concentrations of PDA and P-dots were carefully modulated so that only empty PDA nanoparticles (either micelles or vesicles) and single P-dot-embedded PDA nanoparticles were formed (*vide infra*). After that, the empty PDA nanoparticles, free DAs, or any aggregates formed during the processes of encapsulation were then separated by use of a 0.2  $\mu\text{m}$  membrane filter and size-exclusion chromatography in sequence.

**Fluorescence Spectra of NIR Dyes and PF-BT-DBT P-Dots.** PF-BT-DBT P-dots exhibit broad absorption bands ranging from 300 to 600 nm (Figure 1A), which is a convenient range for conventional laser excitation and fluorescence microscopy. Besides, the outstanding light-harvesting capacity (i.e., large absorption cross section) and the high fluorescence quantum yield render them extremely bright, that is, roughly 3 orders of magnitude higher than that of typical organic dyes. Moreover, the excellent photostability under aqueous environment, facile surface functionalization, and nontoxicity, along with the aforementioned merits, have demonstrated their usage in diverse biological applications.<sup>36</sup> For the purposes of *in vivo* imaging and diagnosis, however, NIR emissions are greatly desired but the direct synthesis of suitable NIR-fluorescing P-dots remains a tough challenge due to self-quenching issues. Various conventional organic dyes such as the NIR dyes we selected, on the other hand, have shown narrow emission at NIR wavelengths (Figure 1A). Nevertheless, the poor solubility and easy aggregation of conventional NIR dyes in aqueous solutions have hindered their direct employment in biological environment. As a result, the key concept here is to integrate the high absorption cross section offered by P-dots and the narrow emission as well as NIR fluorescence provided by NIR dyes. By directly entrapping NIR dyes into the P-dot matrix, followed by PDA capping processes as described above, we were able to obtain the resulting nanoparticles with hydrodynamic diameters of 33, 29, and 34 nm for the NIR653-,

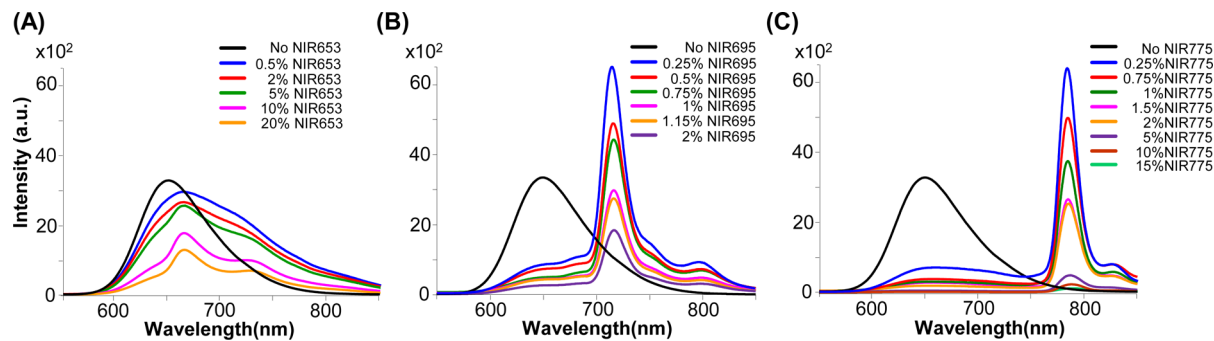


**Figure 2.** Fluorescence spectra of (A) NIR653-, (B) NIR695-, and (C) NIR775-doped PF-BT-DBT P-dots at different doping concentrations (w/w).

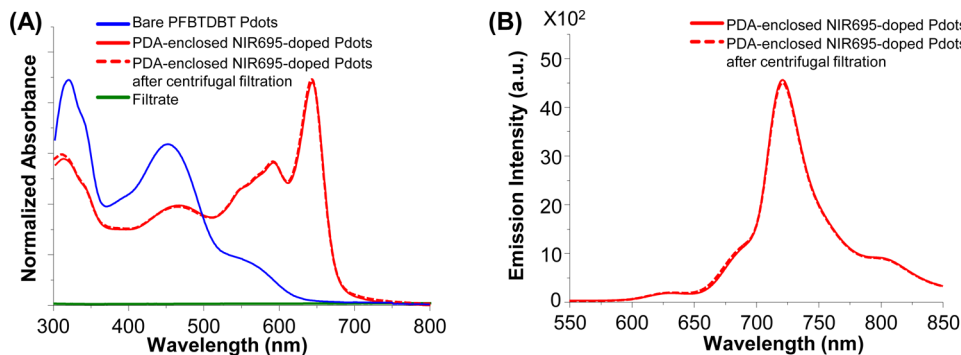


**Figure 3.** Studies of stability of PDA-enclosed NIR695-doped PF-BT-DBT P-dots. (A) Absorption spectra of NIR695-PF-BT-DBT P-dot solution before (red solid line) and after (red dashed line) centrifugal filtration. The green solid line shows absorption of the filtrate, indicating no leaching of NIR695 dyes from the PF-BT-DBT P-dot matrix. (B) Emission spectra of NIR695-PF-BT-DBT P-dot solution before (red solid line) and after (red dashed line) centrifugal filtration further confirmed no leakage of NIR dyes from PDA-coated P-dots.

NIR695-, and NIR775-doped P-dots, respectively (Figure 1B–D). We also noticed that the particle sizes of these dye-doped P-dots increased only ~7 nm after PDA encapsulation, demonstrating that only a single layer of PDA was capped onto the dye-doped P-dots. The sizes of the NIR dye-doped P-dots were not affected or only minimally affected by the doping concentrations.

**Modulating Optical Properties of P-Dots.** As shown in Figure 2, we found that either NIR695 or NIR775 could efficiently quench the PF-BT-DBT emission even at low concentrations, but NIR653 showed less efficiency of energy transfer from P-dot to NIR dyes. We then focused on careful optimization of the ratios of polymer/NIR695 and polymer/NIR775 and found that the ideal doping concentrations are 0.25–0.75% (w/w) for NIR695 and 0.25–1% (w/w) for NIR775 (Figure 2B,C). Considering that the subsequent PDA encapsulation processes including vigorous sonication, heating, and photopolymerization might lose very small amount of NIR dyes, we fine-tuned the polymer/dye ratio in order to have an optimal fluorescence intensity of the NIR dye while minimizing the emission intensity of the polymer. We found that doping 0.75% NIR695 or 1% NIR775 into the P-dot matrix, respectively, could have the optimal optical performance and photostability (*vide infra*). At these doping concentrations, we estimated that there were ~83 NIR695 dyes and ~94 NIR775 dyes per P-dot, respectively. The molecular weight of PF-BT-DBT we synthesized here (Scheme S1, Supporting Information) was determined to be ~12 300 by gel-permeation chromatography (GPC), which means there were ~650 and ~1000 polymer chains condensed inside each NIR695- and NIR775-embedded P-dot, respectively. Based on this informa-

tion, the numbers of polymers per NIR dye was calculated to be ~8 and ~11 for 0.75% NIR695-doped and 1% NIR775-doped P-dots, respectively. The encapsulation efficiency was also calculated to be ~80% (Figure S2, Supporting Information). These resulting NIR-emitting P-dots possessed large Stokes shift that greatly reduced the cross-talk between excitation source and NIR fluorescence emission and offered narrow emission for multiplexed applications.

**Stability of PDA-Capped NIR-Emitting P-Dots.** For practical applications and translation of the NIR-emitting P-dots for widespread adoption, the optical stability of the NIR-entrapped P-dot solution is important. Besides, surface functionalization of these dye-doped P-dots is prerequisite for further bioconjugation. Usually the surface functionalization of P-dots relies on the blending of an amphiphilic nonfluorescent polystyrene polymer, PS-PEG-COOH, where the hydrophilic poly(ethylene glycol) (PEG) chains terminated with carboxylic acid tend to extend into aqueous environment for further chemical reactions. However, more than 50% (w/w) of PS-PEG-COOH needed to be blended into each individual P-dot in order to prevent the leaching of entrapped dyes from the P-dot matrix,<sup>6</sup> which greatly reduced the per-particle fluorescence brightness. To circumvent this problem while at the same time providing functional groups onto P-dots, here we capped the surface of P-dots with carboxylic acid-terminated diacetylenes and then proceeded with polymerization to form PDAs that acted as a fence to trap the doped dyes. As shown in Figure 3A, the emergence of a new absorption band at ~650 nm demonstrated the formation of ordered and fully conjugated PDAs.<sup>56,54</sup> This  $\pi-\pi^*$  transition peak shifts to ~550 nm once the average conjugation length is reduced due to structural

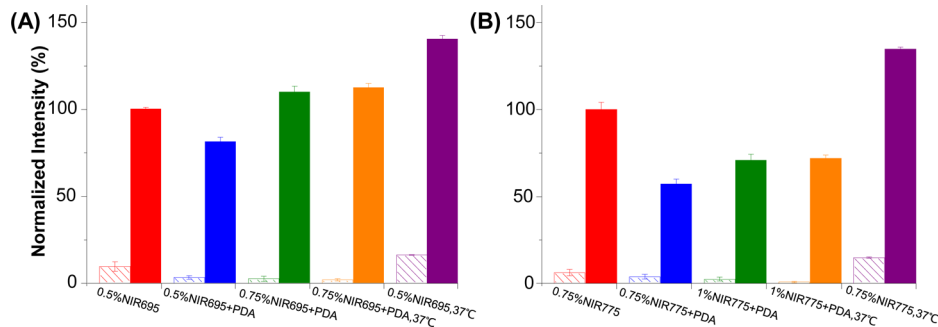


**Figure 4.** Studies of potential leakage of NIR dye dopant from PF-BT-DBT P-dots. Normalized fluorescence intensities of (A) NIR695- and (B) NIR775-doped PFBTDBT P-dots under different experimental conditions are shown.

disturbance or strain.<sup>56</sup> We then conducted a dye leaching test by spinning the PDA-capped PF-BT-DBT–NIR695 P-dot solution in a centrifugal filtration device (Amicon Ultra-4 centrifugal filter with a molecular weight cutoff of 100 000) at a speed of 5000 rpm for 2 min. We then measured the absorption spectra of the P-dot–NIR695 solution after centrifugal filtration and of the filtrate. Negligible change in the absorption of P-dot–NIR695 solution (red dashed line in Figure 3A) and absence of the NIR dye peak from the filtrate (green solid line in Figure 3A) demonstrated that no leaching of the embedded NIR695 dyes from PF-BT-DBT–NIR695 P-dots occurred during this centrifugal process. The unchanged fluorescence spectra of PF-BT-DBT–NIR695 P-dots before and after centrifugal filtration (Figure 3B) further indicated that the PDA coating was highly stable and permanent. The high stability of these PDA-enclosed P-dots was not observed for the traditional physical blending method as reported elsewhere.<sup>42</sup>

We also evaluated the P-dot stability in physiological conditions. As shown in Figure 4A, initially we doped only 0.5% NIR695 into the P-dot matrix, but we found that the emission intensity of NIR695 (red solid column) decreased after PDA polymerization (blue solid bar), suggesting that part of NIR695 dyes might degrade during photopolymerization. To compensate for this photodegradation, we raised the doping concentration of NIR695 to 0.75% and found that the emission intensity of NIR695 could be maintained at the same or even a bit higher level after polymerization (green solid bar). We then evaluated the optical stability of these 0.75% NIR695-doped P-dots by incubating the P-dot solution at 37 °C for 24 h. We observed no noticeable change in the emission intensities of either NIR dyes (orange solid bar) or PF-BT-DBT polymer (orange striped bar). On the other hand, drastic increases in the emission intensities of both NIR dyes (purple solid bar) and PF-BT-DBT (purple striped bar) for the 0.5% NIR695-doped P-dots without PDA entrapment were seen. This indicated that the lack of PDA coating led to leakage of doped NIR dyes from the P-dot matrix and thus decreased energy transfer from the P-dot to the dyes. Similar results were also observed for PF-BT-DBT–NIR775 P-dots (Figure 4B), which further confirmed that the PDA capping layer on the surface of dye-doped P-dots could efficiently seal the embedded dyes inside the P-dot matrix and thereby promote optical stability of the dye-doped P-dots. It is worth mentioning that NIR775 dyes are subject to photodegradation much more easily than NIR695 dyes (compare blue, green, and orange bars in Figure 4 panels A and B). Therefore, we focused on development of NIR695-doped P-dots in the following bioconjugation and sensing experiments.

### Fluorescence Enhancement and Calculation of Förster Radius for Polymer–NIR Dye Pair.

As summarized in Table 1, fluorescence quantum yields of all three NIR dye-

**Table 1. Summary of Fluorescence Quantum Yields of NIR Dyes and NIR Dye-Doped PF-BT-DBT P-Dots**

doped dyes	NIR653	NIR695	NIR775
NIR dyes <sup>a</sup>	0.061	0.088	0.060
NIR dye-doped PF-BT-DBT P-dots (NIR dye emission) <sup>b</sup>	0.225	0.222	0.201
NIR dye-doped PF-BT-DBT P-dots (PF-BT-DBT emission) <sup>c</sup>	0.031	0.042	0.029

<sup>a</sup>In tetrahydrofuran (THF) solution. Each NIR dye was excited at its maximum absorption wavelength. <sup>b</sup>In aqueous solution. Emission in the range 700–850 nm was collected at  $\lambda_{ex} = 450$  nm. <sup>c</sup>In aqueous solution. Emission in the range 600–700 nm was collected at  $\lambda_{ex} = 450$  nm, while the quantum yield of bare PF-BT-DBT P-dots was determined to be 30%.

doped PF-BT-DBT P-dots ( $\lambda_{ex} = 450$  nm) in the range 700–850 nm were greatly enhanced as compared to those of free NIR dyes in THF ( $\lambda_{ex} = 653$ , 695, and 775 nm for NIR653, NIR695, and NIR775, respectively). In the meantime, quantum yields of NIR dye-doped PF-BT-DBT P-dots ( $\lambda_{ex} = 450$  nm) in the range 600–700 nm were significantly reduced as compared to that of nondoped PF-BT-DBT P-dots. This large fluorescence enhancement was attributed to the high light-harvesting capability of PF-BT-DBT and the efficient energy transfer from polymer to NIR dyes. The phenomenon could also be observed by exciting the NIR695-doped PF-BT-DBT P-dots at 450 nm, in which more than 20 times emission enhancement was seen as compared to the emission intensity when excited at 695 nm (Figure S3, Supporting Information).

We also calculated the Förster radius for polymer–NIR dye pair using the FRET system (see Supporting Information). Figure 1A shows the degree of spectral overlap between PF-BT-DBT emission and NIR695 absorption. On the basis of this information, we calculated that  $J$  was  $\sim 1.3 \times 10^{14} \text{ M}^{-1} \cdot \text{cm}^{-1} \text{nm}^4$  by use of eq S3 (Supporting Information). The corresponding Förster radius,  $R_o$ , was determined to be  $\sim 3.3$  nm by use of eq S2 (Supporting Information).

Using a time-correlated single-photon counting module system, we determined the fluorescence lifetime ( $\tau$ ) of PF-BT-DBT P-dots to be 4.98 ns, while the lifetime of 0.75% NIR695-doped PF-BT-DBT P-dots was shortened to 1.02 ns (Figure 5A). Experimentally, the change in P-dot lifetime suggests a FRET efficiency of 80%, which is fairly close to the FRET efficiency of 78% estimated from steady-state quenching.

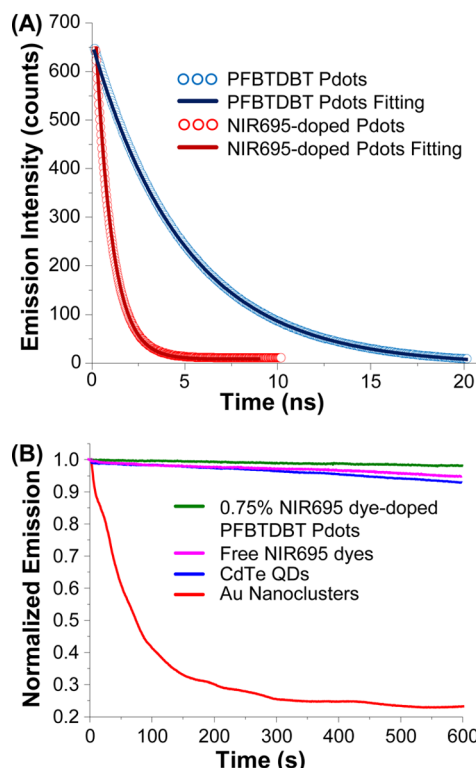


**Figure 5.** (A) Time-resolved fluorescence decay of bare PF-BT-DBT P-dots (experimental data, blue circles; fitting, blue solid line) and 0.75% NIR695-doped PFBTDBT P-dots (experimental data, red circles; fitting, red solid line). (B) Photostability (normalized fluorescence intensity vs time) of 0.75% NIR695-doped PF-BT-DBT P-dots (green curve), free NIR695 dyes (purple curve), CdTe QDs (blue curve), and Au nanoclusters (red curve) in bulk aqueous solutions (except free NIR695 dyes, which were in THF). Three photobleaching trajectories were obtained under the same experimental conditions (380 nm excitation from a 150 W CW xenon lamp) at the same concentration of 4 pM.

To calculate the FRET efficiency by use of eq S1 (Supporting Information), we have to calculate the distance ( $r$ ) between the donor and the acceptor first. If we consider a 29 nm 0.75% NIR695-doped PF-BT-DBT P-dot whose density is assumed to be 1 g/cm<sup>3</sup>, the number of PF-BT-DBT polymers is ~650 inside each individual P-dot, and each P-dot contains ~83 NIR695 dyes. Therefore, the average distance between each two neighboring NIR695 molecules is 13 nm, and the average distance ( $r$ ) between each polymer–dye pair is 13/7.8 = 1.7 nm. The FRET efficiency ( $E$ ) can then be calculated from eq

S1 (Supporting Information):  $E = [1 + (1.7/3.3)^6]^{-1} = 98\%$ . Experimentally, we observed a reduced FRET efficiency of 78–80% from the steady-state quenching and lifetime measurements, and we think it might be attributed to the uneven distribution of NIR dyes and/or PF-BT-DBT inside P-dots.

**Photostability of NIR695–PF-BT-DBT P-Dots.** We evaluated the photostability of NIR dye-doped P-dots in comparison with three other fluorescent probes: CdTe quantum dots (QDs), Au nanoclusters, and NIR dyes. As shown in Figure 5B, all of the four probes were photobleached in the same experimental conditions (380 nm excitation from a 150 W CW xenon lamp) at the same concentration of 4 pM. The 0.75% NIR695-embedded P-dots exhibited high stability, such that no obvious decrease in the emission intensity was observed during 10 min of xenon light irradiation. On the contrary, the other three probes showed different levels of emission decay after photobleaching for 10 min. These results indicated that the host P-dot matrix helped stabilize NIR695 and showed improved photostability over other fluorescent probes.

**Labeling of Cellular Targets with 0.75% NIR695–PF-BT-DBT P-Dots.** To demonstrate the applicability of these NIR-embedded P-dots for cellular labeling, we introduced them into HeLa cells via endocytosis without any additional reagents. After the P-dots were taken up by cells, we washed the cells thoroughly with phosphate-buffered saline (PBS) and then fixed the cells with 4% paraformaldehyde for 15 min. Figure 6 shows confocal fluorescence microscopy images of HeLa cells after the endocytosis of P-dots. The NIR fluorescence signals (Figure 6B) clearly revealed that the PF-BT-DBT–NIR695 P-dots accumulated inside the endosomes or lysosomes, demonstrating that these PDA-coated PF-BT-DBT–NIR695 P-dots remained intact even after being transferred into the acidic environment involved in endocytosis.

As mentioned above, the carboxyl groups on PDAs could be further functionalized for specific cellular targeting. Herein we first conjugated PDA-coated P-dots with streptavidin by 1-ethyl-3-[3-(dimethylamino)propyl]carbodiimide hydrochloride (EDC) catalyzed coupling. The P-dot–streptavidin conjugates, along with primary biotin anti-human CD326 EpCAM antibody, were then incubated with MCF-7 breast cancer cells. As shown in Figure 7A, the P-dot–streptavidin probes could be effectively labeled on the surfaces of MCF-7 cells, while negligible fluorescence signal on the cell surface was detected for the negative control sample (Figure 7B), in which no primary biotin anti-human CD326 EpCAM antibody was present. This result proved that the PDA-coated P-dot conjugates exhibited highly specific binding activity with

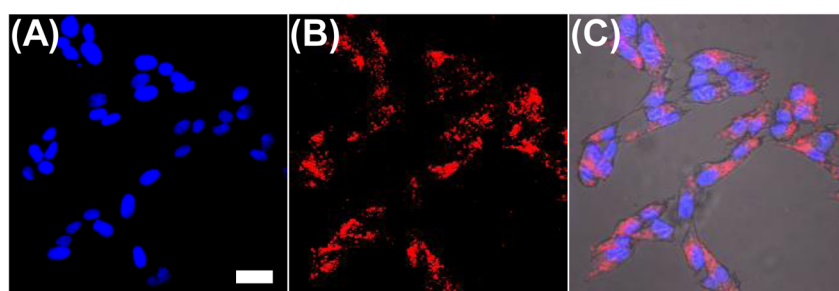


**Figure 6.** Confocal microscopy images of HeLa cells labeled by 0.75% PDA-enclosed NIR695-embedded P-dots through endocytosis. The blue fluorescence shown in panel A is from nuclear counterstain Hoechst 34580, and the red fluorescence shown in panel B is from PDA-coated NIR695-doped P-dots. The image in panel C is the overlay of images A and B and the bright-field image. Scale bar is 30  $\mu$ m.

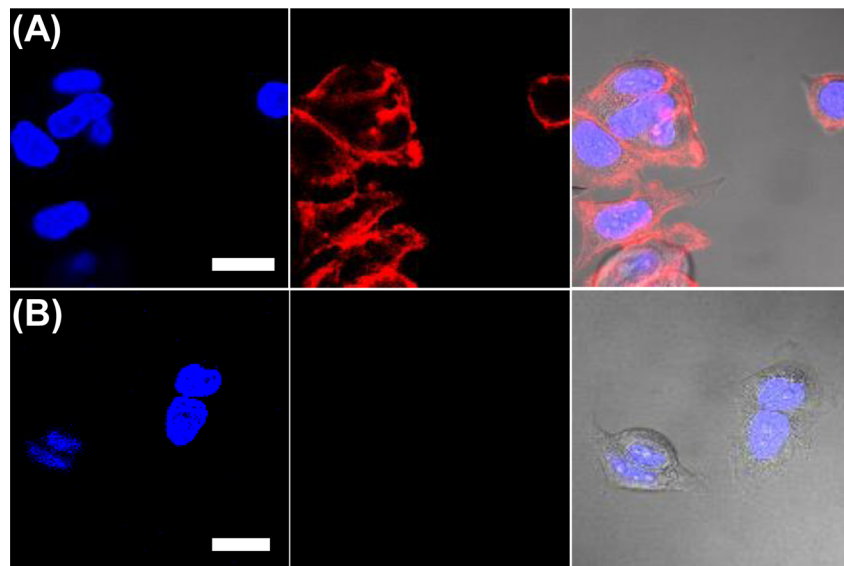


**Figure 7.** Two-color confocal fluorescence images of MCF-7 cells labeled with PF-BT-DBT–NIR695–streptavidin conjugates. (A) Blue fluorescence is from nuclear counterstain Hoechst 34580, and red fluorescence is from NIR695–PF-BT-DBT–streptavidin. The right panel represents fluorescence overlaid with the bright-field image. (B) Images of negative control samples where cells were incubated with PF-BT-DBT–NIR695–streptavidin probes but in the absence of primary biotin anti-human CD326 EpCAM antibody. The scale bars are 20  $\mu$ m.

ultralow nonspecific absorption. We also conducted the same specific cellular labeling with PDA-enclosed bare PF-BT-DBT P-dots as a reference experiment (Figure S4, Supporting Information).

**Proof-of-Concept Sensing Experiment.** To evaluate the feasibility of this system for advanced sensing applications, we conducted a proof-of-concept experiment in which we aimed to create a platform for *in situ* on-site detection. We first prepared a test paper by immersing a filter paper in the concentrated solution of 0.75% NIR695-doped PF-BT-DBT P-dots; the paper was then blown dry with a stream of nitrogen (Figure 8A). Upon exposure to external stimuli, such as heat in this case, the blue-phase PDA underwent a colorimetric transition to its red-phase counterpart. This chromatic change was attributed to a shortening or disturbance of the PDA

conjugation length, and thus we expected the embedded NIR dyes would leach out to give fluorescence recovery of PF-BT-DBT (Figure 8B). It should be noted that red fluorescence on the test paper might partially arise from the red-state PDA but its quantum yield is relatively low (~1%) as compared to that of PF-BT-DBT polymer (~30%). The carboxylic acid groups of PDA can be further fabricated to make the PDA-enclosed P-dots highly sensitive and selective to specific targets. We are now working on surface functionalization of the PDA-enclosed PF-BT-DBT–NIR695 P-dots as a dual-responsive chromophores probe for selective and sensitive detection of ions and biomolecules.

## CONCLUSIONS

In summary, this work describes a facile and scalable method to prepare NIR-fluorescing P-dots emitting at different wavelengths. Using this strategy, we have developed a NIR-emitting P-dot that exhibits much brighter fluorescence than the free NIR dye and possesses narrow emission and a large Stokes shift. The enhanced fluorescence of these NIR dye-doped P-dots was attributed to excellent light-harvesting efficiency and amplified energy-transfer properties of P-dots. More importantly, the optical stability of these NIR-emitting dyes was significantly improved by capping a layer of PDA on the surface of dye-doped P-dots so that no leakage of the embedded dyes from the P-dot matrix was observed. Besides, the coated carboxyl-functionalized PDA layer offered the feasibility for further conjugation and analytical detection. We have demonstrated bioconjugation of the PDA-capped NIR-emitting P-dots and their highly specific binding to both cell surfaces and interiors without any detectable nonspecific binding. In a proof-of-concept experiment, we have created an easy-to-prepare test paper for further on-site detection. We anticipate this new type of PDA-enclosed NIR-emitting P-dots will find broad use both in basic biological studies and in bioimaging and bioanalytical applications. We now focus on the development of a dual-responsive chromophores probe for detection of metal ions using the modified PDA-coated NIR-emitting P-dots.

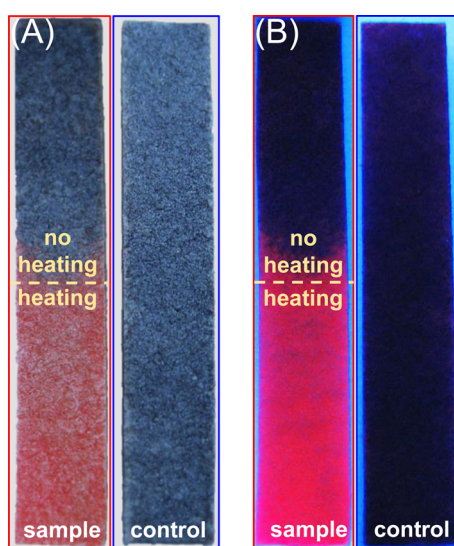


**Figure 8.** Color changes of test paper containing PDA-enclosed PF-BT-DBT–NIR695 P-dots, after immersion into 90 °C hot water for 5 s, under (A) ambient light or (B) 365 nm UV light.

## EXPERIMENTAL SECTION

**Materials.** The following chemicals were purchased from Sigma-Aldrich and used as received: 2,7-dibromofluorene, sodium hydroxide, *tert*-butyl 6-bromohexylcarbamate, tetrahydrofuran (THF; anhydrous,  $\geq 99.9\%$ , inhibitor-free), toluene, tetrabutylammonium bromide ( $Bu_4NBr$ ), phenylboronic acid, bromobenzene, methanol, tetrakis(triphenylphosphine)palladium [ $Pd(PPh_3)_4$ ], dichloromethane ( $CH_2Cl_2$ ), 4,7-dibromobenzo[*c*]-1,2,5-thiadiazole, 9,9-dihexylfluorene-2,7-diboronic acid bis(1,3-propanediol) ester, sodium carbonate, 10,12-pentacosadiynoic acid, selenium dioxide, *o*-phenylenediamine, silver sulfate, and hydrochloric acid. All other chemical reagents were purchased from Invitrogen (Carlsbad, CA) and used as received. High-purity water (18.2 M $\Omega$ ·cm) was used throughout the experiment.

**Preparation of NIR Dye-Doped PF-BT-DBT P-Dots.** Typically, 200  $\mu$ L of PF-BT-DBT (1 mg/mL in THF), 5  $\mu$ L of PS-PEG-COOH (1 mg/mL in THF), and 0–40  $\mu$ L of NIR dyes (1 mg/mL in THF) were added into 5 mL of THF. This mixture was then quickly injected into 10 mL of water under vigorous sonication. THF was then removed by purging with nitrogen on a 96 °C hot plate for 1 h. The resulting P-dot solution was filtered through a 0.2- $\mu$ m cellulose acetate membrane filter to remove any aggregates formed during preparation.

**PDA-Enclosed NIR-Emitting P-Dots.** An aliquot (200  $\mu$ L) of 10,12-pentacosadiynoic acid solution (3 mg/mL in THF) was quickly injected into 3 mL of NIR dye-doped PF-BT-DBT P-dot solution under vigorous sonication. The mixture was further sonicated for 10 min and then THF was removed at 60 °C for 30 min. The solution was then cooled at 4 °C for 2 h. After that, the coated diacetylenes were polymerized upon exposure to a 254 nm UV lamp for 15 min under nitrogen atmosphere. The empty PDA nanoparticles, free DAs, and any aggregates formed during the processes of encapsulation were separated by use of a 0.2  $\mu$ m membrane filter and size-exclusion chromatography (Sephadex HR-300 gel medium, molecular mass cutoff  $1.5 \times 10^6$  Da) in sequence.

**Bioconjugation of PDA-Enclosed NIR-Emitting P-Dots.** Bioconjugation was performed via the EDC-catalyzed reaction between carboxylate-functionalized PDA-coated NIR-emitting P-dots and the respective amine-containing streptavidin. In a typical bioconjugation reaction, 80  $\mu$ L of poly(ethylene glycol) (5% w/v PEG, MW 3350) and 80  $\mu$ L of concentrated *N*-(2-hydroxyethyl)piperazine-*N'*-ethanesulfonic acid (HEPES) buffer (1 M) were added to 4 mL of P-dot solution, resulting in a P-dot solution in 20 mM HEPES buffer with a pH of 7.3. Then 240  $\mu$ L of streptavidin (1 mg/mL) was added to the solution and it was mixed well on a vortex mixer. After that, 80  $\mu$ L of freshly prepared EDC solution (5 mg/mL in Milli-Q water) was added to the solution, and the mixture was stirred for 4 h at room temperature. After bioconjugation, 80  $\mu$ L of bovine serum albumin (BSA, 10 wt %) was added to the P-dot solution and the reaction was continued for another 20 min. An 80- $\mu$ L aliquot of Triton X-100 in Milli-Q water (2.5 wt %) was added to the P-dot-streptavidin mixture. The mixture was then transferred to a centrifugal ultrafiltration tube (Amicon Ultra-4, molecular mass cutoff 100 kDa) and concentrated to 0.5 mL by centrifugation. Finally, the P-dot-streptavidin bioconjugates were purified by gel filtration on Sephadex HR-300 gel medium.

## ASSOCIATED CONTENT

### S Supporting Information

Additional text, three equations, one scheme, and four figures with details of synthetic procedures of PFBTDBT and screening of various NIR dye-doped P-dots. This material is available free of charge via the Internet at <http://pubs.acs.org>.

## AUTHOR INFORMATION

### Corresponding Author

\*E-mail [yhchan@mail.nsysu.edu.tw](mailto:yhchan@mail.nsysu.edu.tw).

### Notes

The authors declare no competing financial interest.

## ACKNOWLEDGMENTS

We thank the Ministry of Science (101-2113-M-110-015-MY2), NSYSU-KMU Joint Research Project (103-I 004), and National Sun Yat-sen University. We also gratefully acknowledge support for this research from Professors Chao-Ming Chiang, Wei-Lung Tseng, and Chin-Hsing Chou and Dr. Jiun-Yi Shen from National Taiwan University, and we thank the Instrumentation Center at National Sun Yat-sen University for use of instruments.

## REFERENCES

- (1) Robinson, E. H.; Gowda, A. S. P.; Spratt, T. E.; Gold, B.; Eichman, B. F. *Nature* **2010**, *468*, 406.
- (2) Rosenfeld, N.; Young, J. W.; Alon, U.; Swain, P. S.; Elowitz, M. B. *Science* **2005**, *307*, 1962.
- (3) Kotecha, N.; Flores, N. J.; Irish, J. M.; Simonds, E. F.; Sakai, D. S.; Archambeault, S.; Diaz-Flores, E.; Coram, M.; Shannon, K. M.; Nolan, G. P.; Loh, M. L. *Cancer Cell* **2005**, *14*, 335.
- (4) Frangioni, J. V. *J. Clin. Oncol.* **2008**, *26*, 4012.
- (5) van Dam, G. M.; Themelis, G.; Crane, L. M. A.; Harlaar, N. J.; Pleijhuis, R. G.; Kelder, W.; Sarantopoulos, A.; de Jong, J. S.; Arts, H. J. G.; van der Zee, A. G. J.; Bart, J.; Low, P. S.; Ntzachristos, V. *Nat. Med.* **2011**, *17*, 1315.
- (6) Jin, Y.; Ye, F.; Zeigler, M.; Wu, C.; Chiu, D. T. *ACS Nano* **2011**, *5*, 1468.
- (7) Yuan, L.; Lin, W.; Zhao, S.; Gao, W.; Chen, B.; He, L.; Zhu, S. *J. Am. Chem. Soc.* **2012**, *134*, 13510.
- (8) Mok, H.; Jeong, H.; Kim, S.-J.; Chung, B. H. *Chem. Commun.* **2012**, *48*, 8628.
- (9) Reul, R.; Tsapis, N.; Hillaireau, H.; Sancey, L.; Mura, S.; Recher, M.; Nicolas, J.; Coll, J.-L.; Fattal, E. *Polym. Chem.* **2012**, *3*, 694.
- (10) Yang, Y.; An, F.; Liu, Z.; Zhang, X.; Zhou, M.; Li, W.; Hao, X.; Lee, C.-s.; Zhang, X. *Biomaterials* **2012**, *33*, 7803.
- (11) Schönbächler, A.; Glaied, O.; Huwyler, J.; Frenz, M.; Pieles, U. *J. Photochem. Photobiol., A* **2013**, *261*, 12.
- (12) Peng, J.; He, X.; Wang, K.; Tan, W.; Wang, Y.; Liu, Y. *Anal. Bioanal. Chem.* **2007**, *388*, 645.
- (13) Peng, H.-s.; Stolwijk, J. A.; Sun, L.-N.; Wegener, J.; Wolfbeis, O. S. *Angew. Chem., Int. Ed.* **2010**, *49*, 4246.
- (14) Mader, H. S.; Kele, P.; Saleh, S. M.; Wolfbeis, O. S. *Curr. Opin. Chem. Biol.* **2010**, *14*, 582.
- (15) Medintz, I. L.; Uyeda, H. T.; Goldman, E. R.; Mattoussi, H. *Nat. Mater.* **2005**, *4*, 435.
- (16) Somers, R. C.; Bawendi, M. G.; Nocera, D. G. *Chem. Soc. Rev.* **2007**, *36*, 579.
- (17) Choi, H. S.; Liu, W.; Misra, P.; Tanaka, E.; Zimmer, J. P.; Ipe, B. I.; Bawendi, M. G.; Frangioni, J. V. *Nat. Biotechnol.* **2007**, *25*, 1165.
- (18) Michalet, X.; Pinaud, F. F.; Bentolila, L. A.; Tsay, J. M.; Doose, S.; Li, J. J.; Sundaresan, G.; Wu, A. M.; Gambhir, S. S.; Weiss, S. *Science* **2005**, *307*, 538.
- (19) Derfus, A. M.; Chan, W. C. W.; Bhatia, S. N. *Nano Lett.* **2004**, *4*, 11.

- (20) Brunetti, V.; Chibli, H.; Fiammengo, R.; Galeone, A.; Malvindi, M. A.; Vecchio, G.; Cingolani, R.; Nadeau, J. L.; Pompa, P. P. *Nanoscale* **2013**, *5*, 307.
- (21) Sapsford, K. E.; Pons, T.; Medintz, I. L.; Mattoussi, H. *Sensors* **2006**, *6*, 925.
- (22) Krauss, T. D.; Peterson, J. J. *Nat. Mater.* **2012**, *11*, 14.
- (23) Bottrell, M.; Green, M. *Chem. Commun.* **2011**, *47*, 7039.
- (24) Hoshino, A.; Hanada, S.; Yamamoto, K. *Arch. Toxicol.* **2011**, *85*, 707.
- (25) Ghaderi, S.; Ramesh, B.; Seifalian, A. M. *J. Drug Targeting* **2011**, *19*, 475.
- (26) Wu, C.; Bull, B.; Szymanski, C.; Christensen, K.; McNeill, J. *ACS Nano* **2008**, *2*, 2415.
- (27) Tian, Z.; Yu, J.; Wu, C.; Szymanski, C.; McNeill, J. *Nanoscale* **2010**, *2*, 1999.
- (28) Pecher, J.; Mecking, S. *Chem. Rev.* **2010**, *110*, 6260.
- (29) Kaeser, A.; Schenning, A. P. H. J. *Adv. Mater.* **2010**, *22*, 2985.
- (30) Tuncel, D.; Demir, H. V. *Nanoscale* **2010**, *2*, 484.
- (31) Li, K.; Liu, B. *J. Mater. Chem.* **2012**, *22*, 1257.
- (32) Pu, K.-Y.; Liu, B. *Adv. Funct. Mater.* **2011**, *21*, 3408.
- (33) Wu, C.; Chiu, D. T. *Angew. Chem., Int. Ed.* **2013**, *52*, 3086.
- (34) Chen, C.-P.; Wu, P.-J.; Liou, S.-Y.; Chan, Y.-H. *RSC Adv.* **2013**, *3*, 17507.
- (35) Wu, C.; Jin, Y.; Schneider, T.; Burnham, D. R.; Smith, P. B.; Chiu, D. T. *Angew. Chem., Int. Ed.* **2010**, *49*, 9436.
- (36) Wu, C.; Schneider, T.; Zeigler, M.; Yu, J.; Schiro, P. G.; Burnham, D. R.; McNeill, J. D.; Chiu, D. T. *J. Am. Chem. Soc.* **2010**, *132*, 15410.
- (37) Wu, C.; Hansen, S. J.; Hou, P. Q.; Yu, J.; Zeigler, M.; Jin, Y.; Burnham, D. R.; McNeill, J. D.; Olson, J. M.; Chiu, D. T. *Angew. Chem., Int. Ed.* **2011**, *50*, 3430.
- (38) Chan, Y.-H.; Wu, C.; Ye, F.; Jin, Y.; Smith, P. B.; Chiu, D. T. *Anal. Chem.* **2011**, *83*, 1448.
- (39) Chan, Y.-H.; Jin, Y.; Wu, C.; Chiu, D. T. *Chem. Commun.* **2011**, *47*, 2820.
- (40) Ye, F.; Wu, C.; Jin, Y.; Chan, Y.-H.; Zhang, X.; Chiu, D. T. *J. Am. Chem. Soc.* **2011**, *133*, 8146.
- (41) Harbron, E. J.; Davis, C. M.; Campbell, J. K.; Allred, R. M.; Kovary, M. T.; Economou, N. J. *J. Phys. Chem. C* **2009**, *113*, 13707.
- (42) Yu, J.; Wu, C.; Zhang, X.; Ye, F.; Gallina, M. E.; Rong, Y.; Wu, I.-C.; Sun, W.; Chan, Y.-H.; Chiu, D. T. *Adv. Mater.* **2012**, *24*, 3498.
- (43) Chan, Y.-H.; Gallina, M. E.; Zhang, X.; Wu, I.-C.; Jin, Y.; Sun, W.; Chiu, D. T. *Anal. Chem.* **2012**, *84*, 9431.
- (44) Chan, Y.-H.; Ye, F.; Gallina, M. E.; Zhang, X.; Jin, Y.; Wu, I.-C.; Chiu, D. T. *J. Am. Chem. Soc.* **2012**, *134*, 7309.
- (45) Sun, W.; Hayden, S.; Jin, Y.; Rong, Y.; Yu, J.; Ye, F.; Chan, Y.-H.; Zeigler, M.; Wu, C.; Chiu, D. T. *Nanoscale* **2012**, *4*, 7246.
- (46) Wu, P.-J.; Chen, J.-L.; Chen, C.-P.; Chan, Y.-H. *Chem. Commun.* **2013**, *49*, 898.
- (47) Zhang, X.; Yu, J.; Rong, Y.; Ye, F.; Chiu, D. T.; Uvdal, K. *Chem. Sci.* **2013**, *4*, 2143.
- (48) Koehorst, R. B. M.; Fokkink, R. G.; Stuart, M. C.; Zuilhof, H.; Sudholter, E. J. R. *Macromolecules* **2002**, *35*, 4226.
- (49) Ahn, D. J.; Chae, E.-H.; Lee, G. S.; Shim, H.-Y.; Chang, T.-E.; Ahn, K.-D.; Kim, J.-M. *J. Am. Chem. Soc.* **2003**, *125*, 8976.
- (50) Mosley, D. W.; Sellmyer, M. A.; Daida, E. J.; Jacobson, J. M. *J. Am. Chem. Soc.* **2003**, *125*, 10532.
- (51) Yang, Y.; Lu, Y.; Lu, M.; Huang, J.; Haddad, R.; Xomeritakis, G.; Liu, N.; Malanoski, A. P.; Sturmayr, D.; Fan, H.; Sasaki, D. Y.; Assink, R. A.; Shelnutt, J. A.; Swol, F. v.; Lopez, G. P.; Burns, A. R.; Brinker, C. J. *J. Am. Chem. Soc.* **2003**, *125*, 1269.
- (52) Duan, L.; Garrett, S. J. *Langmuir* **2001**, *17*, 2986.
- (53) Yam, C. M.; Dickie, A. J.; Kakkar, A. K. *Langmuir* **2002**, *18*, 8481.
- (54) Chan, Y.-H.; Lin, J.-T.; Chen, I.-W. P.; Chen, C.-h. *J. Phys. Chem. B* **2005**, *109*, 19161.
- (55) Wu, J.; Zawistowski, A.; Ehrmann, M.; Yi, T.; Schmuck, C. J. *Am. Chem. Soc.* **2011**, *133*, 9720.
- (56) Chen, X.; Zhou, G.; Peng, X.; Yoon, J. *Chem. Soc. Rev.* **2012**, *41*, 4610.
- (57) Yarimaga, O.; Jaworski, J.; Yoon, B.; Kim, J.-M. *Chem. Commun.* **2012**, *48*, 2469.